Journal of Nuclear Medicine, published on December 1, 2016 as doi:10.2967/jnumed.116.180158

Synthesis and evaluation of the new estrogen receptor β selective radioligand ^{18}F-FHNP: comparison with ^{18}F-FES

Inês F. Antunes[1]*, Aren van Waarde[1], Rudi A.J.O Dierckx[1], Elisabeth G.E. de Vries[2], Geke A.P. Hospers[2] and Erik F.J. de Vries[1]

[1]Dept. of Nuclear Medicine and Molecular Imaging, University of Groningen, University Medical Center Groningen, Groningen, The Netherlands

[2] Dept. of Medical Oncology, University of Groningen, University Medical Center Groningen, Groningen, The Netherlands

* Author for correspondence:

Inês F. Antunes, Department of Nuclear Medicine and Molecular Imaging, University Medical Center Groningen, University of Groningen, PO Box 30.001, 9700 RB Groningen, The Netherlands, Tel.: +31-50-3615779, FAX: +31-50-3611687, Email: i.farinha.antunes@umcg.nl

Running title: ^{18}F-FHNP for ER-β expression

Word count: 4943

ABSTRACT

Estrogen receptors (ER) are targets for endocrine treatment of estrogen-dependent cancers. The ER consists of 2 isoforms, ERα and ERβ, which have distinct biological functions. While activation of ERα stimulates cell proliferation and cell survival, ERβ promotes apoptosis. Positron emission tomography (PET) of ERα and ERβ levels could provide more insight in response to hormonal treatment. 16α-^{18}F-Fluoro-17β-estradiol (^{18}F-FES) is a PET tracer for ER with relative selectivity for ERα. Here we report the synthesis and evaluation of a potential ERβ-selective PET tracer: 2-^{18}F-fluoro-6-(6-hydroxynaphthalen-2-yl)pyridin-3-ol (^{18}F-FHNP). **Methods:** ^{18}F-FHNP was synthesized by fluorination of the corresponding nitro precursor, followed by acidic removal of the 2-methoxyethoxymethyl protecting group. *In-vitro* affinity of ^{18}F-FHNP and ^{18}F-FES for ER was evaluated in SKOV3 ovarian carcinoma cell. PET imaging and *ex-vivo* biodistribution studies with ^{18}F-FHNP and ^{18}F-FES were conducted in athymic nude mice bearing a SKOV3 xenograft. **Results:** FHNP has nanomolar afffinty for ERs, with a 3.5 times higher affinity for ERβ. ^{18}F-FHNP was obtained in 15-40% radiochemical yield (decay-corrected) with a specific activity of 279±75 GBq/μmol. ^{18}F-FHNP had a K_D of 2 nM and B_{max} of 18 fmol/10^6 cells, while ^{18}F-FES had a K_D of 3 nM and B_{max} 83 fmol/10^6 SKOV3 cells. Both ^{18}F-FHNP and ^{18}F-FES PET could clearly visualize the tumor in male mice bearing a SKOV3 xenograft. Biodistribution studies showed similar distribution of ^{18}F-FHNP and ^{18}F-FES in most peripheral organs. ^{18}F-FES showed 2-fold higher tumor uptake than ^{18}F-FHNP. The tumor-to-plasma ratio of ^{18}F-FES decreased 55% (p=0.024) and 8% (p=0.68) when administered in the presence of estradiol (non-selective) and genistein (ERβ-selective), respectively. The tumor-to-plasma ratio of ^{18}F-FHNP decreased 47% (p=0.004) and 70% (p=0.0009) when administered with estradiol and genistein, respectively. **Conclusion:** The new

PET tracer ^{18}F-FHNP has suitable properties for imaging and shows relative selectivity for ERβ.

Keywords: Estrogen receptors, hormones, PET, imaging, cancer

INTRODUCTION

Estrogens play a central role not only in the growth, development and maintenance of a diverse range of healthy tissues, but also in hormone-regulated cancers, including breast, ovarian and prostate cancers (*1*). The effects of estrogens are mediated through two receptors, estrogen receptor α (ERα) and β (ERβ), which operate as ligand-dependent transcription factors that modulate oncogenesis and tumor suppressor gene activation. Inhibition of hormone receptor signaling can be an effective treatment in hormone-regulated cancer (*2*), provided that these receptors are actually expressed by the tumors .

ERα and ERβ have distinct biological functions and their levels can vary in both normal tissue and tumors. While ERβ is expressed in breast, ovarian and prostate tissues, ERα is usually the major subtype in cancers derived from these organs, with ERβ levels decreasing as the cancer progresses (*3*). In general, activation of ERα by estrogens stimulates cell proliferation and cell survival in tumors. While, signaling via the ERβ is thought to be anti-proliferative and to promote apoptosis in cancer, since ERβ can inhibit ERα signaling by forming ERα-ERβ heterodimers (*4*). Because of the opposite effects induced by ERα and ERβ, a tool to determine the ER phenotype of all tumors in the body would be of great interest. Currently, ER expression and phenotype are usually determined ex-vivo in a biopsy of the primary tumor. However, ER status of metastases may differ from the primary tumor. In addition, receptor expression by the tumor can change over time, either spontaneously or due to treatment. Crosstalk of the ER with the growth factor receptors is an important factor leading to the treatment-induced changes in ER expression (*5,6*).

PET can non-invasively generate whole body images of receptor expression and thus can be used to monitor the ER status of all tumor lesions in a patient. The images could guide clinicians in therapeutic decision-making. Currently, 17β-^{18}F-fluoro-16α-estradiol is used as a

PET tracer for clinical assessment of the ER status in patient with a clinical dilemma (*7,8*). In a high percentage of the patients, ^{18}F-FES-PET actually caused a change in treatment regimen, indicating that ER imaging can indeed have an important impact on patient management (*8*). However, ^{18}F-FES possesses a weak subtype selectivity (ERα/ERβ=2.5) (*9*). Therefore, ^{18}F-FES-PET can provide accurate information about ER expression, but not about the ER phenotype. Subtype-selective tracers would allow the assessment of the ERβ/ERα ratio offering a better characterization of tumor lesions and therefore, a better assessment of the stage of the disease and its sensitivity towards different endocrine therapies. Most importantly, the ER-β subtype tracers could be used in the assessment of the ER-β in lung carcinomas (*10*) and lung fibrosis (*11*)where it is known to be involved in these diseases . Unfortunately, PET tracers with high subtype-selectivity for ERβ or ERα are currently unavailable.

Recently, Harris *et al.* reported a series of phenylnaphthalene compounds with good ERβ/ERα selectivity (*12*). Based on the properties of this series of phenylnaphthalene analogues, we selected 6-(3-fluoro-4-hydroxyphenyl)naphthalene-2-ol, with an ERβ/ERα selectivity of 17, as a lead compound for development of a PET tracer for ERβ imaging.

Radiolabeling of this compound for PET imaging could theoretically be achieved by a nucleophilic aromatic substitution reaction of the corresponding aromatic nitro or quaternary ammonium compound with ^{18}F-fluoride. However, this reaction only proceeds well if the electron density of the benzene ring is sufficiently reduced by a strong electron-withdrawing group. Unfortunately, our lead compound does not contain electron-withdrawing substituents and therefore, cannot be labeled in this manner. Nowadays, several new approaches are in development that would allow direct fluorination of electron-rich aromatic rings, using for example iodonium salts, sulfonium salts and boronic acids (*13,14*). On the other hand, nucleophilic aromatic fluorination reactions of 2-nitropyridines with ^{18}F-fluoride are facile and

give high labeling yields (*15*). We selected this strategy as first approach to develop a PET tracer for ERβ. Therefore, the pyridine analogue of our lead compound, 6-(3-fluoro-4-hydroxyphenyl)naphthalene-2-ol (FHNP), was selected as candidate PET tracer for ERβ imaging. Herein, we describe the synthesis and biological evaluation of ^{18}F-FHNP (Fig. 1).

MATERIALS AND METHODS

The synthesis and characterization of unlabeled FHNP and the nitro precursor (Supplemental Figs. 1 and 2) are presented in supplemental materials (available at http://jnm.snmjournals.org).

^{18}F-FES was produced as previously described (*16*). The lipophilicity $LogD_{7.4}$ studies were performed as previously described (*17*).

The *in vitro* binding affinity of FHNP towards ERα and ERβ (*18*) was determined by a competitive radiometric binding assay using ^{3}H-estradiol as the ligand (Supplemental Table 1).

PET image reconstruction, data analysis and ex-vivo biodistribution was performed as previously described (*19*). Tracer uptake was expressed as %ID/g.

The western blotting was performed according to the literature (*20*).

Radiosynthesis of ^{18}F-FHNP

Aqueous ^{18}F-fluoride was produced by irradiation of ^{18}O-water with a Scanditronix MC-17 cyclotron via the $^{18}O(p,n)^{18}F$ nuclear reaction. The ^{18}F-fluoride solution was passed through a QMA SepPak Light anion exchange cartridge (Waters) to recover the ^{18}O-water. The ^{18}F-fluoride was eluted from the cartridge with 1 mL of K_2CO_3 (5 mg/mL) and collected in a vial with 15 mg kryptofix[2.2.2]. To this solution, 1 mL acetonitrile was added and the solvents were evaporated at 130 ^{o}C. The ^{18}F-KF/kryptofix complex was dried 3 times by the addition of 0.5 mL acetonitrile, followed by evaporation of the solvent. A solution of 3-((2-

methoxyethoxy)methoxy)-6-(6-((2-methoxyethoxy)methoxy)naphthalene-2-yl)-2-nitropyridine (1 mg, 2.1 mmol) in 0.5 mL of dry dymethylsulfoxide was added to the ^{18}F-KF/kryptofix complex. The reaction mixture was heated at 150 ^{o}C for 15 min. After the mixture was allowed to cool down to 90 ^{o}C , 1 mL 2M HCl was added and the reaction mixture was heated at 90 ^{o}C for 15 min to remove the 2-methoxyethoxymethyl groups. The product was purified by high-performance liquid chromatography (Column: Luna C18;5µm, 250×4.6 mm, eluent: 30% acetonitrile in 0.025M phosphate buffered saline, pH=7; flow: 4 mL/min; retention time ^{18}F-FHNP =24 min). The radioactive peak corresponding to the product was collected and diluted with 50 mL of distilled water and passed through a C18 SepPak light cartridge (Waters, conditioned with 5 mL ethanol and 10 mL water). The product was eluted from the cartridge with 0.7 mL ethanol, followed by 5 mL distilled water. Quality control was performed by ultra-performance liquid chromatography, using a HSS T3 column (1.8 µm, 3.0x50 mm) with 30% aqueous acetonitrile as mobile phase at a flow of 1 mL/min (retention time: ^{18}F-Fluoride=0.5 min, ^{18}F-FHNP =2.1 min).

Stability of ^{18}F-FHNP

Samples of ^{18}F-FHNP dissolved in formulated eluent (1 mL) were analyzed after 60 minutes at room temperature by ultra-performance liquid chromatography (see above).

Animals

Athymic male nude mice (6-8 weeks old, n=36, Harlan, The Netherlands) were used to avoid high variability of endogenous estradiol levels. All studies were carried out in compliance with the Dutch regulations for animal experiments. The protocol was approved by the Institutional Animal Care and Use Committee (protocol number: DEC 6657A). After one week of acclimatization, SKOV3 cells [1 to 2×10^{6} cells in a 1:1 mixture of Matrigel and Dulbecco's

Modified Eagle's Medium-high with 10% fetal bovine serum] were subcutaneously injected into the upper back of the mice. When palpable tumor nodules were formed the animals were divided in 2 groups: i) injected with ^{18}F-FES and ii) injected with ^{18}F-FHNP

Pet Imaging in Mice Bearing a Skov3 Xenograft

On day 15 after SKOV3 cell inoculation, the mice were anesthetized with 2% Isoflurane, positioned in the center of the field-of-view of the small animal PET camera (Focus 220, Siemens-Concorde) in a transaxial position. ^{18}F-FES (14±7 MBq) or ^{18}F-FHNP (9±4 MBq) were either mixed with Phosphate buffer saline (control) or estradiol (non-selective ER ligand, 0.3 µg/g animal) and injected via the penile vein of the animal. In a subset of control animals, genistein (ERβ-selective ligand, 5 µg/g animal) was intraperitoneally administered 5 min before tracer injection. Simultaneously with the injection of the PET tracer, a 60-min dynamic emission scan was started. After the PET scan was completed, a 15-min transmission scan with a Co-57 point source was obtained for the correction of scatter and attenuation of 511 keV photons by tissue. Once the transmission scan was concluded, the animals were terminated with an overdose of anesthesia. The animals remained fixed to the bed and transferred on the bed to the computed tomography (CT) scanner (MicroCT II, CTI Siemens). A 15-min CT scan was acquired for anatomic localization of the tumor (19)

Immunohistochemistry

Formalin-fixed, paraffin-embedded SKOV3 tumor sections were deparaffinized in xylene, rehydrated, incubated overnight with the rabbit monoclonal anti-ERα (ab32063) or mouse monoclonal anti-ERβ (ab16813) primary antibody. The next day the slides were incubated with a secondary biotinylated antibody. 3,3'-Diaminobenzidine tetrahydrochloride for the visualization of the antibody/enzyme complex. The counterstaining was performed with

hematoxylin/blue reagent. Positive cells present a brownish color while negative controls and unstained cells become blue.

Statistical Analysis

` The K_D, B_{max} and the IC_{50} values were determined with GraphPad Prism 5.04 (GraphPad software). Differences in tracer accumulation between groups were analyzed using the two-sided unpaired students´ t-test. Significance was reached when $p<0.05$. Data are presented as mean ± standard deviation unless stated otherwise.

RESULTS

Radiochemistry

^{18}F-FHNP was obtained in 15-40% radiochemical yield (decay-corrected) within 130 min . At the end of synthesis, the specific activity was 279±75 GBq/µmol and the radiochemical purity was always higher than 95%. ^{18}F-FES was obtained in 15±8% decay-corrected radiochemical yield. Specific activity of ^{18}F-FES was 244±112 GBq/µmol, with a radiochemical purity of 99.9±0.2%. ^{18}F-FHNP and ^{18}F-FES were stable for at least 60 min, as no decomposition was observed by ultra-performance liquid chromatography analysis. The distribution coefficients (logD, octanol/phosphate buffer pH 7.4) of ^{18}F-FHNP and ^{18}F-FES were 1.85±0.01 and 2.50±0.01, respectively.

In-vitro binding affinity

The *in-vitro* binding affinity of ^{18}F-FHNP and ^{18}F-FES towards ER was evaluated in ER-negative MDA-MB-231 and ER-positive SKOV3 cells (Fig. 2), using different concentrations of the competitive inhibitor estradiol. The estradiol concentration that inhibited

50% of tracer binding (IC_{50}) was 8.5 pM and 8.3 pM for ^{18}F-FHNP and ^{18}F-FES in SKOV3 cells, respectively.

When SKOV3 cells were incubated with increasing amounts of ^{18}F-FHNP and ^{18}F-FES, saturation curves were obtained. The Scatchard plot obtained from these saturation curves (Fig. 3) provided a dissociation constant (K_D) of 2 nM and maximum binding capacity (B_{max}) of 18 fmol/10^6 cells for ^{18}F-FHNP and a K_D of 3 nM and B_{max} 83 fmol/10^6 cells for ^{18}F-FES.

The in-vitro selectivity of FHNP towards ERα and ERβ was determined by a competitive radiometric binding assay using ^{3}H-estradiol as the ligand (*18*). The binding affinities of FHNP for ERα and for ERβ were 1.5% and 5.2% relative to estradiol. Thus, FHNP showed an approximately 3.5 times higher selectivity for ERβ than for ERα in this assay (supplemental Table 1).

^{18}F-FES binding assays in SKOV-3 cells with different concentrations of subtype-selective ligands gave comparable IC_{50} values for the ERα antagonist fulvestrant (6.8 pM) (*21*) and the ERβ agonist genistein (8.5 pM) (*22*). When ^{18}F-FHNP was used as the radioligand, a 5-fold higher IC_{50} value (38 pM) was obtained for fulvestrant, whereas a 10-fold lower IC_{50} value (0.8 pM) was observed for genistein (Supplemental Fig. 3).

In-vivo Pet Imaging

^{18}F-FHNP and ^{18}F-FES PET scans were performed in SKOV3 tumor-bearing athymic nude mice that were injected with vehicle or with the ER ligands estradiol or genistein (Fig. 4). The time activity curves of the tumors revealed faster kinetics for ^{18}F-FHNP than for ^{18}F-FES. The accumulation of ^{18}F-FHNP in the tumors of control mice reached a maximum 2.5 min post-injection and subsequently decreased exponentially with a half-life of 20±4 min. In contrast, the accumulation of ^{18}F-FES in the tumors of control mice reached a maximum 10 min post-

injection and afterwards decreased exponentially with a half-life of 60±30 min. The tracer accumulation in tumors obtained from the last 10 min of the PET scan (50-60 min) were 0.86±0.18 %ID/g for ^{18}F-FES and 0.21±0.03 %ID/g for ^{18}F-FHNP. Injection of ^{18}F-FES together with estradiol resulted in a significant reduction in tumor uptake (0.38±0.18 %ID/g, $p<0.05$), whereas genistein did not significantly affect ^{18}F-FES uptake (0.73±0.12 %ID/g, $p=0.33$). Likewise, estradiol – but not genistein – significantly reduced the area under the time-activity curve of the tumor ($p=0.048$) (Supplemental Fig. 4). Tumor uptake of ^{18}F-FHNP, on the other hand, was significantly decreased by both estradiol (0.12±0.07 %ID/g, $p<0.05$) and genistein (0.15±0.01 %ID/g, $p<0.05$). The area under the curve, however, was only significantly reduced by genistein ($p=0.033$).

Ex-vivo Biodistribution

In SKOV3 xenograft-bearing mice, ^{18}F-FHNP exhibited a similar biodistribution as ^{18}F-FES in most peripheral organs, with the highest uptake in liver, kidneys and urine at 1h post-injection (Figs. 5 and 6). ^{18}F-FES showed approximately 2 times higher tumor uptake (1.32±0.66 %ID/g) than ^{18}F-FHNP (0.57±0.07 %ID/g) (Supplemental Tables 2 and 3). ^{18}F-FHNP uptake in the excised tumors was significantly lower in animals that were injected with estradiol (0.45±0.10 %ID/g, $p<0.05$) or genistein (0.30±0.08 %ID/g, $p<0.001$). In contrast, ^{18}F-FES uptake in the excised tumors was only significantly reduced in animals that were co-injected with estradiol (0.56±0.35 %ID/g, $p<0.05$), but not in mice that were injected with genistein (1.11±0.39 %ID/g, $p=0.52$). Likewise, the tumor-to-plasma ratio of ^{18}F-FHNP (0.60±0.12) was significantly reduced after injection with estradiol (0.29±0.11, $p<0.01$) or genistein (0.20±0.06, $p<0.001$), whereas the tumor-to-plasma ratio of ^{18}F-FES (1.16±0.48) was only significantly reduced when co-injected with estradiol (0.53±0.22, $p<0.05$).

Immunohistochemistry

To confirm the expression of both ER subtypes in SKOV3 xenografts, tumors were sectioned and stained for ERα and ERβ expression. As shown in Fig. 7, the SKOV3 tumors express both ERα and ERβ, although ERα is more abundant than ERβ.

Western blotting

Western blotting was performed to evaluate the ERα and ERβ expression in the SKOV3 xenografts. Immunoreactive bands for ERα and ERβ were visualized at 65KDa and 55 KDa, respectively (Supplemental Fig. 5). As shown in Fig. 7D, SKOV3 tumors express significantly higher amounts of ERα than ERβ ($p=0.048$).

DISCUSSION

Selective PET imaging of ERβ or ERα expression in endocrine tumors may provide a useful molecular assessment of the stage of the disease and its sensitivity towards various endocrine therapies and therefore might help in the selection of the most appropriate therapies for each individual patient. In this study, we developed the fluorine-18 radioligand, ^{18}F-FHNP for imaging ERβ and compared it to the standard PET tracer ^{18}F-FES, which is known for its preferential affinity towards ERα.

The optimized radiolabeling of ^{18}F-FHNP consisted on a one-pot two-step fluorination-deprotection procedure, which lead to the desired product with similar specific activity as ^{18}F-FES. Although ^{18}F-FHNP does not possess a steroidal structure, it was found that it has a lipophilicity (1.85±0.01) similar to ^{18}F-FES (2.50±0.01).

Besides being stable, having adequate lipophilicity and high specific activity, a suitable PET tracer must also have high affinity towards ER, and, in this case, high selectivity towards

ERβ. Thus, in order to evaluate ^{18}F-FHNP affinity towards ER and compare it to ^{18}F-FES, a competitive radiometric binding assay was performed with both tracers in SKOV3 (ER-positive) and MDA-MB-231 (ER-negative) cells. As expected, ^{18}F-FHNP and ^{18}F-FES binding were displaced by estradiol only in SKOV3 cells, demonstrating that ^{18}F-FHNP and ^{18}F-FES have affinity towards the total ER population. This was further confirmed with a Scatchard plot, providing similar dissociation constants in a nanomolar range for both tracers. However, Bmax obtained for ^{18}F-FHNP in SKOV3 cells was 5-fold lower than for ^{18}F-FES. This low Bmax value obtained for ^{18}F-FHNP may be explained by the low levels of ERβ, which was confirmed by immunohistochemistry and western blotting.

To confirm ERβ-selectivity, a binding assay was performed with ERα and ERβ using ^{3}H-estradiol as the ligand, showing a 3.5 times higher selectivity of FHNP for ERβ. This value is lower than the reported value for 6-(3-fluoro-4-hydroxyphenyl)-naphthalene-2-ol (ERβ/ERα=17), indicating that the substitutions of the phenyl ring with a pyridine ring may have decreased the selectivity of FHNP for ERβ.

In an attempt to further prove the ERβ-selectivity of ^{18}F-FHNP , different subtype-selective ligands were used in a competitive binding assay. As depicted in Supplemental Fig. 3, genistein competes stronger (lower IC_{50}) with ^{18}F-FHNP than with ^{18}F-FES, whereas fulvestrant competes stronger with ^{18}F-FES than with ^{18}F-FHNP. This is in agreement with ^{18}F-FES being more selective for the same subtype as fulvestrant (ERα) and ^{18}F-FHNP being more selective for the same subtype as genistein (ERβ).

To evaluate the potential of ^{18}F-FHNP as a PET tracer for in-vivo imaging of ERβ expression, dynamic PET scans were performed in the SKOV3 tumor-bearing athymic nude mice. The SKOV3 tumors can grow independent of endogenous or exogenous estradiol, because SKOV3 xenografts are known to express human epidermal growth factor receptor-2 in

addition to ERα/ERβ and therefore, tumor growth can be stimulated via the express human epidermal growth factor receptor-2 pathway. In fact, we were able to grow SKOV3 xenografts in male athymic nude mice without the use of estrogen pellets. A major advantage of this model is that the levels of circulating estradiol are low and therefore competition of endogenous estradiol with the tracer for the ER binding site is negligible.

The ex-vivo biodistribution studies 1 h post tracer injection showed similar distributions of ^{18}F-FHNP and ^{18}F-FES in most peripheral organs. Uptake in bone was low, indicating minimal defluorination for both tracers. The highest tracer accumulation for both tracers was in the excretion organs. The accumulation of ^{18}F-FHNP in urine was 3 times higher than ^{18}F-FES, while similar radioactivity levels were found in other excretion organs (liver and kidneys) for both tracers. The higher accumulation of ^{18}F-FHNP in the urine can be attributed to the lower lipophilicity of ^{18}F-FHNP, resulting in less non-specific binding and faster renal clearance. This could also explain the 2 times lower tumor accumulation of ^{18}F-FHNP when compared to ^{18}F-FES. results obtained from PET imaging (Fig. 4) were similar to those obtained from ex-vivo biodistribution.

The time activity curves of control mice revealed that tumor washout of ^{18}F-FHNP was faster than the tumor clearance of [^{18}F]FES. However, one cannot ascribe the faster tumor washout of ^{18}F-FHNP with certainty to a lower *in-vivo* affinity of the tracer for the ER receptors than ^{18}F-FES, since tumor uptake is also determined by other factors, like receptor expression levels, tracer delivery and nonspecific binding. In fact, immunuhistochemistry and western blotting (Fig. 7) revealed that the SKOV3 xenografts have lower expression of ERβ than ERα, which is in agreement with literature data (*23*). With less binding sites available for a ERβ-selective tracer, the retention of ^{18}F-FHNP is indeed expected to be less than the retention of the ERα-selective tracer ^{18}F-FES.

To investigate the specificity of tracer uptake in ER-positive tumors *in-vivo*, binding sites were saturated by administration of the non-selective ER ligand estradiol or the ERβ-selective compound genistein. Injection of ^{18}F-FES with estradiol resulted in a significant reduction in tumor uptake, whereas genistein did not significantly affect ^{18}F-FES uptake. As genistein is an ERβ-selective ligand, it binds less to ERα and as a result it cannot compete with ^{18}F-FES binding to ERα. Given the low ERβ expression levels in SKOV3 xenografts, the reduction in ^{18}F-FES uptake after administration of genistein is expected to be less pronounced than the reduction in the tumor uptake when the tracer is co-injected with estradiol. Tumor uptake of ^{18}F-FHNP, on the other hand, was significantly decreased by both estradiol and genistein suggesting that ^{18}F-FHNP is predominantly bound to ERβ in SKOV3 xenografts *in vivo*.

Interestingly, animals which were injected with ER blockers had significantly higher plasma levels of ^{18}F-FHNP, which eventually leads to higher tracer delivery of the tracer to the tumor. Nevertheless, a significant reduction of ^{18}F-FHNP uptake in tumors was found after injection of an ER-blocker, which clearly shows that ^{18}F-FHNP has high affinity towards ER and, more particularly towards ERβ, as tumor to plasma ratio decreased by 70% ($p<0.001$).

There have been several attempts to develop an ERβ PET tracer (*9*,*24*). Perhaps the most relevant one was ^{18}F-FEDPN with a RBA of 8% for ERβ and a relative selectivity ERβ/ERα of 20 (*9*). Although our PET tracer, ^{18}F-FHNP, have lower RBA and selectivity than ^{18}F-FEDPN we were still able to observe modest blocking effects in this study. Most likely due to the higher levels of ER in our target compared to the uterus and ovaries used in previous studies. In addition, the low defluorination of our compound might have also influenced the selective uptake by increasing tracer delivery over time

Although this study was performed with a SKOV3 human ovarian carcinoma cell line, it does not give any guaranties that the PET tracer will also work in a clinical setting. Therefore, these data need to be confirmed in other studies, preferably in models with higher ERβ expression such as genetically engineered cell lines expressing only ERβ. If successful, clinical trials are warranted to assess the potential clinical usefulness of ^{18}F-FHNP.

CONCLUSION

^{18}F-FHNP can be readily radiolabeled with fluorine-18 in high yield, providing a product with high specific activity. *In-vitro* binding studies indicated that ^{18}F-FHNP has a higher affinity towards ERβ than ERα. PET imaging studies show that ERβ expressing tumors can be clearly visualized with ^{18}F-FHNP PET. Moreover, *in-vivo* studies with ^{18}F-FHNP confirm that the tracer has a preferential affinity towards ERβ. These promising preclinical results warrant further preclinical and clinical studies to confirm whether this PET tracer is indeed suitable for ERβ imaging.

DISCLOSURE

This study was funded by Mammoth project of the Center for Translational Molecular Medicine (CTMM). No other potential conflict of interest relevant to this article was reported.

AKNOWLEDGMENTS

We gratefully thank Dr. H. Timmer for providing the cells and all the advice given during this study; J. Sijbesma, A. Parente and A. Shoji for the help in the in-vivo study, M. Khayum and A. Boerema for all the help with the immunohistochemistry-western blotting assays. We also gratefully thank Dr. F. Marques and Dr. C. Oliveira from Instituto Tecnológico e Nuclear, Portugal, for performing the in-vitro binding assays with ERs.

REFERENCES

1. van Kruchten M, de Vries EG, Brown M, et al. PET imaging of oestrogen receptors in patients with breast cancer. *Lancet Oncol*. 2013;14:e465-e475.

2. Minutolo F, Macchia M, Katzenellenbogen BS, Katzenellenbogen JA. Estrogen receptor β ligands: Recent advances and biomedical applications. *Med Res Rev*. 2011;31:364-442.

3. Fox EM, Davis RJ, Shupnik MA. ERβ in breast cancer-Onlooker, passive player, or active protector? *Steroids*. 2008;73:1039-1051.

4. Pettersson K, Delaunay F , Gustafsson JA. Estrogen receptor bold beta acts as a dominant regulator of estrogen signalling *Oncogene* 2000;19:4970-4978.

5. Marcom PK, Isaacs C, Harris L, et al. The combination of letrozole and trastuzumab as first or second-line biological therapy produces durable responses in a subset of HER2 positive and ER positive advanced breast cancers. *Breast Cancer Res Treat*. 2007;102:43-49.

6. Smith IE, Walsh G, Skene A, et al. A phase II placebo-controlled trial of neoadjuvant anastrozole alone or with gefitinib in early breast cancer. *J Clin Oncol*. 2007;25:3816-3822.

7. van Kruchten M, de Vries EF, Arts HJG, et al. Molecular imaging of ER expression in epithelial ovarian cancer. *J Nucl Med*. 2015;56:50-55.

8. van Kruchten M, Glaudemans AW, de Vries EF, et al. PET imaging of estrogen receptors as a diagnostic tool for breast cancer patients presenting with a clinical dilemma. *J Nucl Med*. 2012;53:182-190.

9. Yoo J, Dence CS,Sharp TL, Katzenellenbogen JA, Welch MJ. Synthesis of an estrogen receptor β-selective radioligand: 5-[18F]Fluoro-(2R*,3S*)-2,3-bis(4-hydroxyphenyl)pentanenitrile and comparison of in vivo distribution with 16α-[18F]Fluoro-17β-estradiol. *J Med Chem*. 2005;48:6366-6378.

10. Niikawa H, Suzuki T, Miki Y, et al. Intratumoral estrogens and estrogen receptors in human non-small cell lung carcinoma. *Clin. Cancer Res*. 2008;14:4417–4426.

11. Taniuchi S, Fujishima F, Miki Y, et al. Tissue concentrations of estrogens and aromatase immunolocalization in interstitial pneumonia of human lung. *Mol Cell Endocrinol.* 2014;392: 136-143.

12. Mewshaw RE, Edsall RJ, Jr., Yang C, et al. ERbeta ligands. 3. Exploiting two binding orientations of the 2-phenylnaphthalene scaffold to achieve ERbeta selectivity. *J Med Chem*. 2005;48:3953-3979.

13. Cole EL, Stewart MN, Littich R, Hoareau R, Scott PJH. Radiosyntheses using Fluorine-18: the art and science of late stage fluorination. *Curr Top Med Chem*. 2014;14:875-900.

14. Mossine AV, Brooks AF, Makaravage KJ, et al. Synthesis of [18F]Arenes via the copper-mediated [18F]fluorination of boronic acids. *Org Lett*. 2015;17:5780-5783.

15. Malik N, Solbach C, Voelter W, Machulla HJ. Nucleophilic aromatic substitution by [18F]fluoride at substituted 2-nitropyridines. *J Radioanal Nucl Chem*. 2010;283:757-764.

16. Römer J, Füchtner F, Steinbach J, Johannsen B. Automated production of 16α-[18F]fluoroestradiol for breast cancer imaging. *J Nucl Med Biol*. 1999;26:473-479.

17. Antunes IF, Haisma HJ, Elsinga PH, Dierckx RA, de Vries EF. Synthesis and evaluation of [18F]-FEAnGA as a PET tracer for beta-glucuronidase activity. *Bioconjug Chem*. 2010;21:911-920.

18. Neto C, Oliveira MC, Gano L, et al. Novel 7alpha-alkoxy-17alpha-(4'-halophenylethynyl)estradiols as potential SPECT/PET imaging agents for estrogen receptor expressing tumours: synthesis and binding affinity evaluation. *Steroids*. 2012;77:1123-1132.

19. Antunes IF, Haisma HJ, Elsinga PH, et al. Induction of β-glucuronidase release by cytostatic agents in small tumors. *Mol Pharm*. 2012;9:3277-3285.

20. Boerema AS. The brain at low temperature: Neuronal & behavioural dynamics in mammalian hibernation and torpor. 2012. http://irs.ub.rug.nl/ppn/340463791

21. Long X, Nephew KP. Fulvestrant (ICI 182,780)-dependentinteracting proteins mediate immobilization and degradation of estrogen receptor. *J Biol Chem.* 2006;.281:9607–9615.

22. Kuiper GG, Carlsson B, Grandien K, et al. Comparison of the ligand binding specificity and transcript tissue distribution of estrogen receptors alpha and beta. *Endocrinology.* 1997;138:863–870

23. O'Donnell AJM, Macleod KG, Burns DJ, Smyth JF, Langdon SP. Estrogen receptor-α mediates gene expression changes and growth response in ovarian cancer cells exposed to estrogen. *Endocrine-Related Cancer*. 2005;12:851-866.

24. Lee JH, Peters O, Lehmann L, et al. Synthesis and biological evaluation of two agents for Imaging estrogen receptor β by positron emission tomography: challenges in PET imaging of a low abundance target. *Nucl Med Biol.* 2012;39:1105-16.

FIGURE LEGENDS

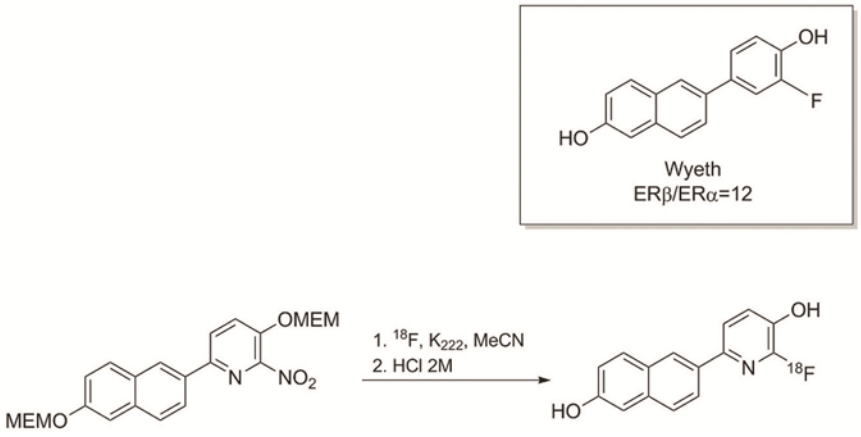

FIGURE 1. Structure of ERβ phenylnaphthalene-core ligand (top). Radiosynthesis of ^{18}F-FHNP (bottom).

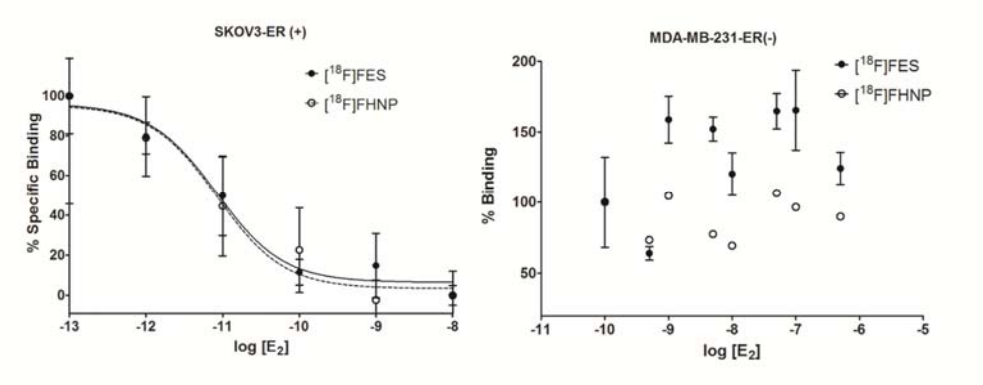

FIGURE 2. In-vitro competitive ER binding assay of ^{18}F-FHNP and ^{18}F-FES in SKOV3 and MDA-MB-231 cells, using estradiol (E2) as the competitor. Data are presented as mean values ± SEM of triplicated samples. Specific binding was obtained by subtracting the non-specific binding (residual binding of the tracer in presence of the highest dose of competing drug) from the total binding, representing 60%-80% of the total uptake by SKOV3 cells

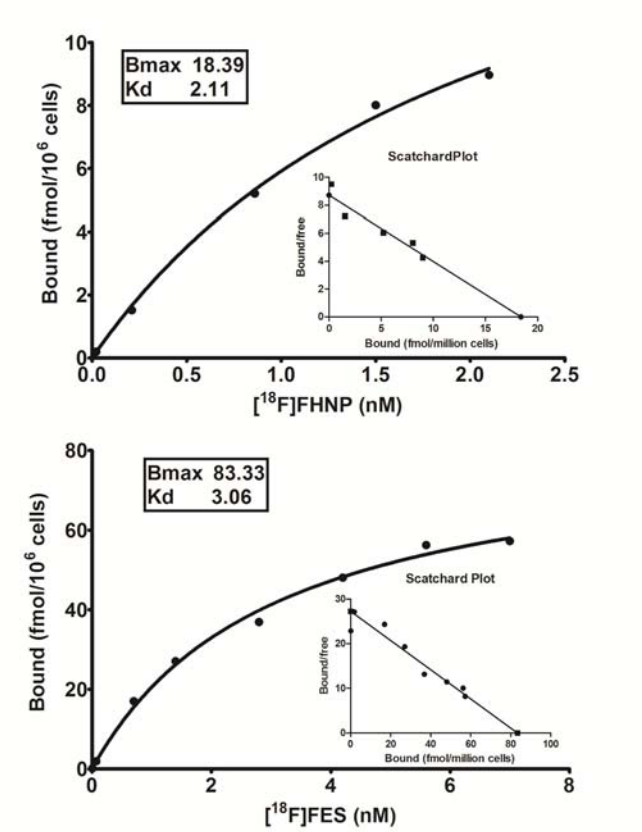

FIGURE 3. Scatchard plots for ^{18}F-FHNP and ^{18}F-FES binding in SKOV3 cells (n=1,triplicate).

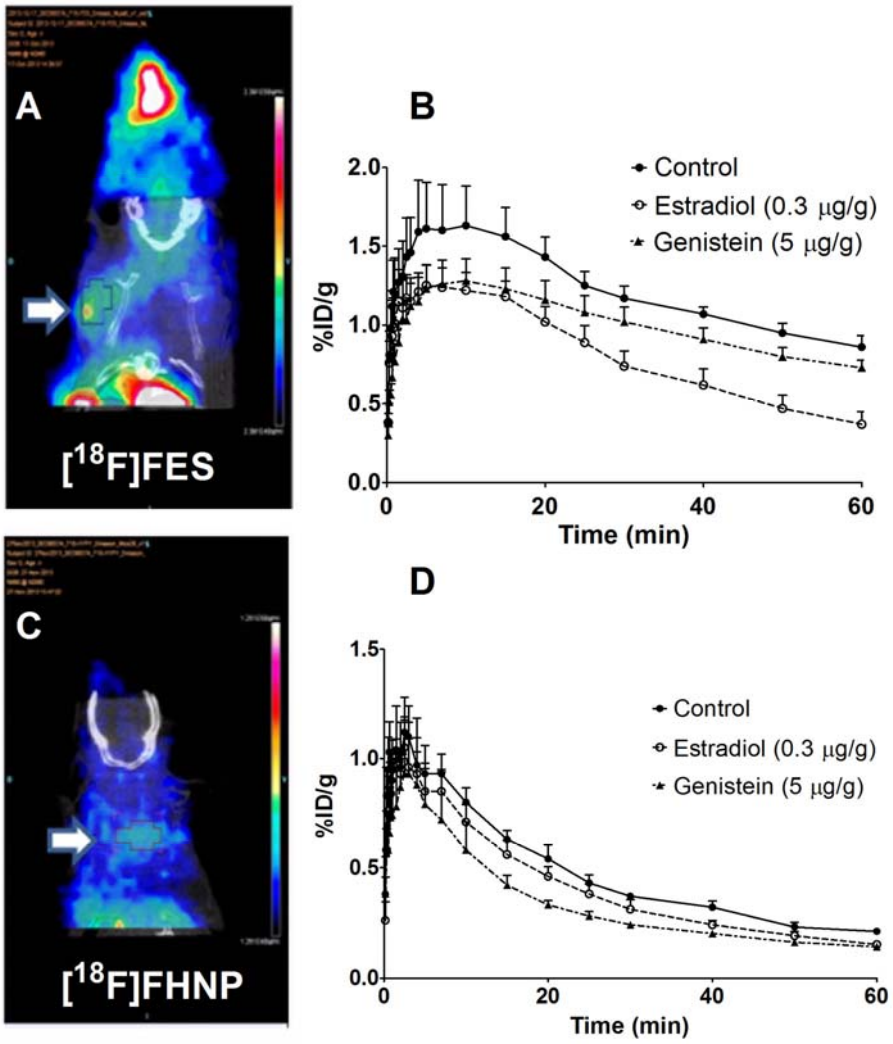

FIGURE 4. Coronal microPET/CT fusion images of 2 mice bearing a SKOV3 xenograft (white arrows) injected with (A) ^{18}F-FES (14±7 MBq) or (C) ^{18}F-FHNP (9±4 MBq). Time activity curves of the tumor uptake (%ID/g) of (B) ^{18}F-FES and(D) ^{18}F-FHNP in SKOV3 xenografts.

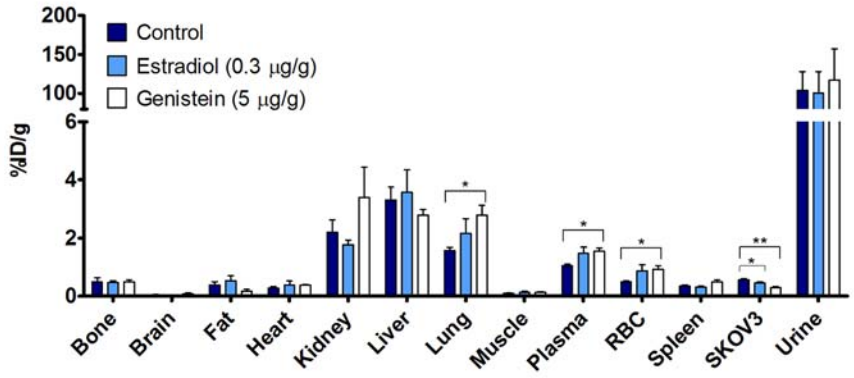

FIGURE 5. Biodistribution 1 h after intravenous injection of ^{18}F-FHNP in mice bearing a SKOV3 tumor xenograft. Competition studies were performed by injection of the tracer with either estradiol (i.v.) or genistein (i.p.). Data are expressed as %ID/g (mean ± SEM). Statistically significant differences between treated and control animals are indicated by asterisks: * $p<0.05$ and ** $p<0.001$.

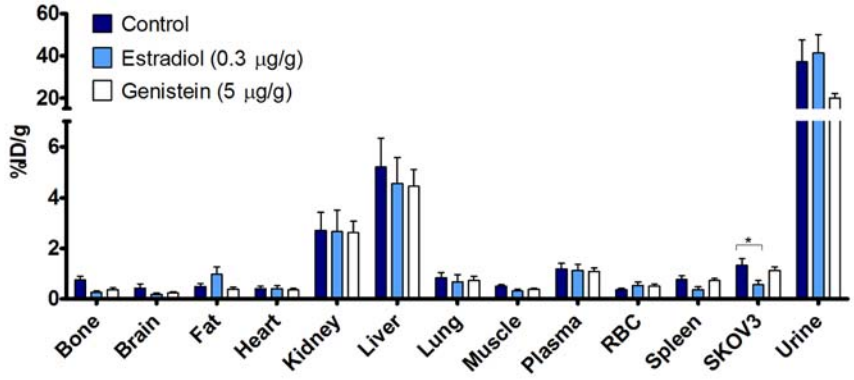

FIGURE 6. Biodistribution 1 h after intravenous injection of ^{18}F-FES in mice bearing a SKOV3 tumor xenograft. Competition studies were performed by injection of the tracer with either estradiol (i.v.) or genistein (i.p.). Data are expressed as %ID/g (mean ± SEM). Statistically significant differences between treated and control animals are indicated by asterisks: * $p<0.05$.

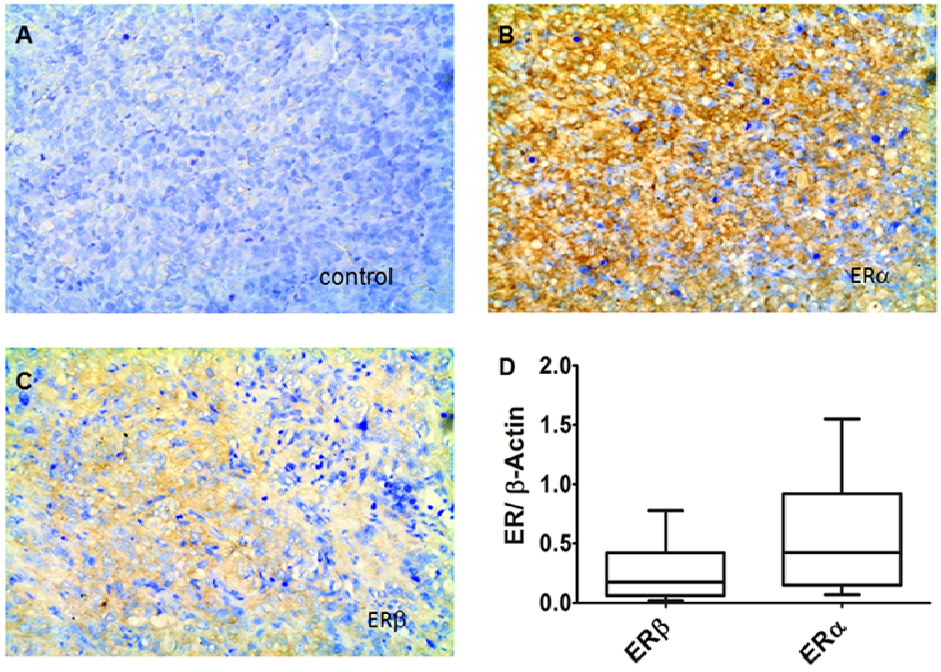

FIGURE 7. Representative immunostaining of SKOV3 xenografts (20x amplification) for: (A) Control (n=1,10 slices); (B) ERα (n=2, 15 slices) and (C) ERβ (n=2, 15 slices). (D) Average Estrogen receptor protein to β-Actin ratio values of a single western blotting experiment (*$p<0.05$).

SUPPLEMENTAL MATERIAL

Chemistry

2-fluoro-6-(6-hydroxynaphthalen-2-yl)pyridine-3-ol (FHNP). A solution of 6-bromo-2-fluoropyridin-3-ol 2 (96 mg, 0.5 mmol), (6-hydroxynaphthalen-2-yl)boronic acid 1 (112 mg, 0.6 mmol), sodium carbonate (1 mL of 2M aqueous, 2 mmol) and tetrakis(triphenylphosphine)palladium (29 mg, 0.025 mmol) in 5 mL dimethoxyethane was stirred under reflux (90 oC) overnight. The reaction mixture was cooled to room temperature, poured into 50 ml of ammonium chloride (1M) and extracted with ethyl acetate. The combined organic layers were washed with water and saturated brine, dried over sodium sulfate, filtered, concentrated and purified by silica gel column chromatography (n-hexane/ethyl acetate 2:1.5) to yield 69 mg (50%) of a beige solid (supplemental Fig. 1). ^{1}H NMR (500 MHz, Chloroform-*d*) δ 8.39 (s, 1H), 8.15 (d, *J* = 2.0 Hz, 2H), 7.82 (d, *J* = 8.9 Hz, 1H), 7.71 (dd, *J* = 8.2, 1.0 Hz, 1H), 7.53 – 7.47 (m, 2H), 7.35 – 7.31 (m, 1H), 5.95 (s, 1H); 256.3 $[M]^+$

6-(6-hydroxynaphthalen-2-yl)-2-nitropyridin-3-ol (compound 5). A solution of 6-bromo-2-nitropyridin-3-ol 4 (220 mg, 1 mmol), (6-hydroxynaphthalen-2-yl)boronic acid 1 (229mg, 1.22mmol), sodium carbonate (2 mL of 2 M aqueous, 4 mmol) and tetrakis(triphenylphosphine)palladium (75 mg, 0.05 mmol) in 8 mL dimethoxyethane was stirred under reflux (90 oC) overnight. The reaction mixture was cooled to room temperature, poured into 50 mL of ammonium chloride (1M) and extracted with ethyl acetate. The combined organic layers were washed with water and brine, dried over sodium sulfate, filtered, concentrated and purified by silica gel column chromatography (n-hexane/ethyl acetate 1:1) to yield 148 mg (52%) of an orange-red solid. . ^{1}H NMR (500 MHz, Chloroform-*d*) δ 10.30 (d, *J* = 6.3 Hz, 1H), 8.50 – 8.41 (m, 2H), 8.28 (dd, *J* = 8.9, 1.7 Hz, 1H), 8.24 – 8.18 (m, 2H), 7.89 (dd, *J* = 15.9, 8.8 Hz, 2H), 7.76 (dd, *J* = 11.4, 8.7 Hz, 1H), 7.35 (d, *J* = 8.9 Hz, 1H), 7.22 – 7.16 (m, 1H); *m/z* 283.1 $[M]^+$

3-((2-methoxyethoxy)methoxy)-6-(6-((2-methoxyethoxy)methoxy)naphthalene-2-yl)-2-nitropyridine (compound 6) Compound 5 (20 mg, 0.07 mmol) was dissolved in dry

dichloromethane and cooled to 0 oC. N,N-diisopropylethylamine (60 µL, 0.34 mmol) was added to this mixture, followed by the slow addition of 2-methoxyethoxymethyl chloride (60 µL, 0.52 mmol). After stirring for 24 h at room temperature, the mixture was washed with saturated ammonium chloride, water and saturated brine. The organic layers were dried over sodium sulfate, filtered and concentrated under reduced pressure. The crude product was purified by column chromatography (hexane/ethyl acetate 1:1) to give 32 mg (63%) of pure product as a yellow solid (supplemental Fig. 2). ^{1}H NMR (500 MHz, Chloroform-d) δ 8.45 – 8.36 (m, 1H), 8.13 – 7.97 (m, 2H), 7.96 – 7.74 (m, 3H), 7.47 (d, *J* = 2.5 Hz, 1H), 7.35 – 7.17 (m, 1H), 5.44 (dd, *J* = 3.1, 0.7 Hz, 4H), 4.02 – 3.79 (m, 4H), 3.70 – 3.47 (m, 4H), 3.50 – 3.25 (m, 6H); *m/z* 459.2 $[M]^{+}$.

In vitro studies

Cells and culture conditions. SKOV3 cells were maintained in Dulbecco's Modified Eagle's Medium-high -high supplemented with 10% fetal calf serum, while MDA-MB-231 (breast carcinoma cells) cells were maintained in Dulbecco's Modified Eagle's Medium-high, supplemented with 10% fetal calf serum and 1 mM glutamine.

In vitro Saturation and competitive binding of 18F-FHNP and 18F-FES. Cells were plated in triplicate in a 24-well plate at a density of 1×105 cells per well. For saturation binding studies, the cells were treated with 50 µL of increasing concentrations of 18F-FES or 18F-FHNP and incubated for 1 hour at 37°C. Since our preliminary cellular uptake studies of 18F-FHNP indicated that its uptake did not increase further at incubation times longer than 10 min (data not shown) further studies were performed with 10 minutes incubation time. Thus, for the competitive studies, 50 µL (1MBq) of 18F-FHNP or 18F-FES solution was added in the absence or presence of different concentrations of estradiol (ERβ and ERα agonist), genistein (ERβ partial agonist) or fulvestrant (ERα antagonist) to SKOV3 cells and incubated for 10 min at 37°C. Afterwards the medium was discarded and the cells were washed with cold PBS, harvested with trypsin and resuspended in DMEM. The cell suspensions were collected from each well and the radioactivity was measured using a gamma counter. The number of viable cells was determined with the trypan blue exclusion technique .

SUPPLEMENTAL FIGURES

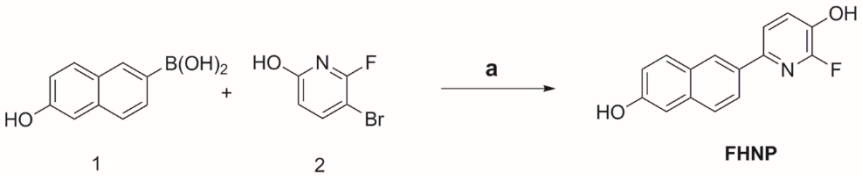

Supplemental Figure 1. Scheme of the synthesis of the reference compound FHNP. Reagents and solvents: Pd(PPh3)4; Na_2CO_3 2M and DME.

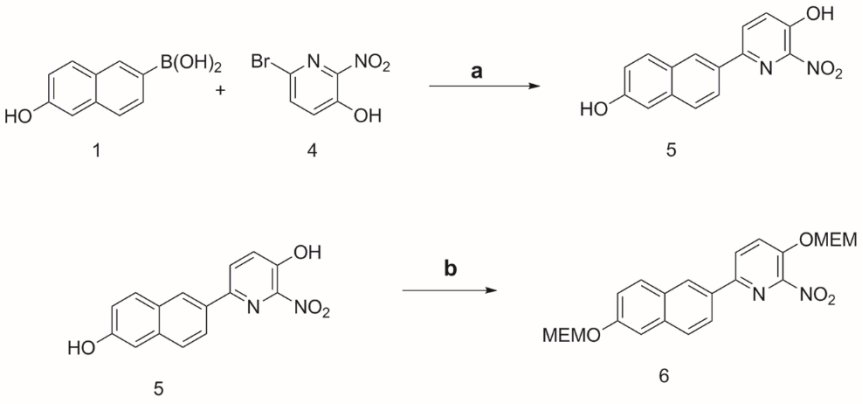

Supplemental Figure 2. Scheme of the synthesis of precursor. Reagents and solvents: a) Pd(PPh3)4, Na_2CO_3 2M and DME; b) MEMCl, DPEA and CH_2Cl_2.

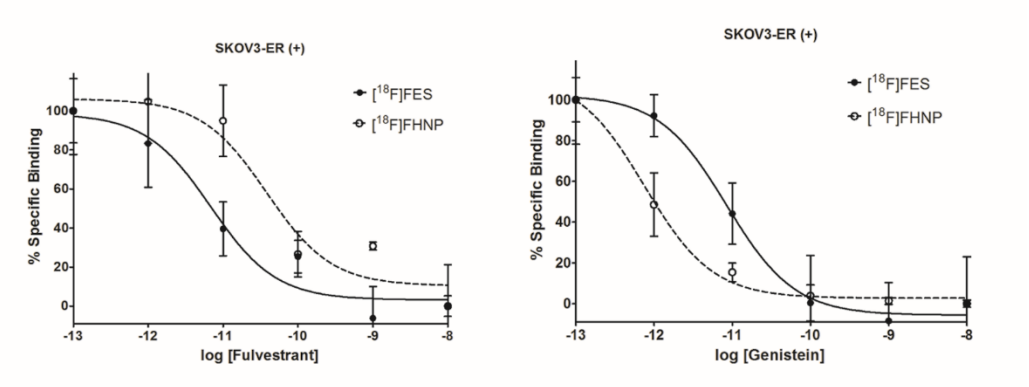

Supplemental Figure 3. In-vitro competitive ER binding assay of ^{18}F-FHNP and ^{18}F-FES in SKOV3 cells, using the ERα-selective ligand Fulvestrant (left) or the ERβ-selective ligand Genistein (right) as the competitor. Data presented in mean values of triplicate samples ± SEM. Specific binding was obtained by subtracting the non-specific binding (residual binding of the tracer in presence of the highest dose of competing drug) from the total binding, representing 60%-80% of the total uptake by cells

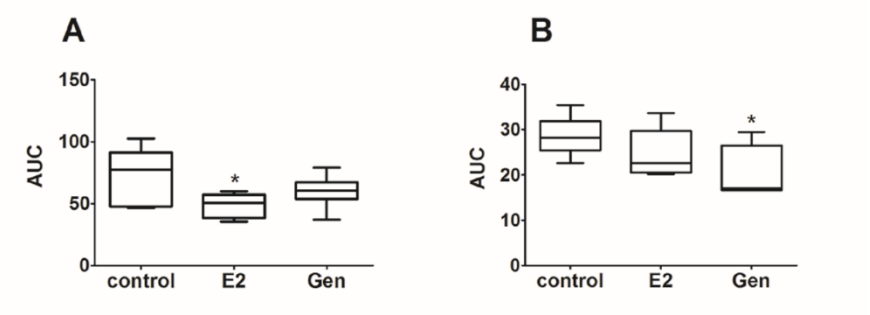

Supplemental Figure 4. Area under the time-activity curve in tumors injected with (A) ^{18}F-FES and (B) ^{18}F-FHNP.

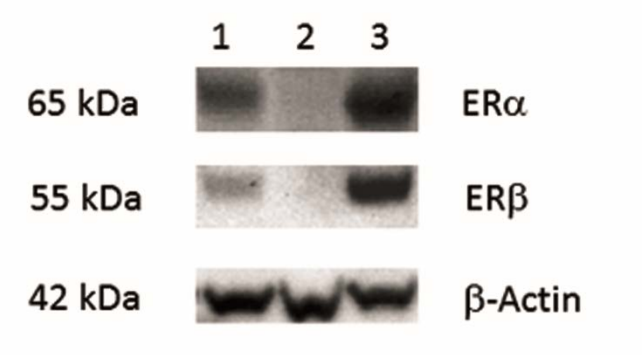

Supplemental Figure 5. A representative image of western blotting performed on SKOV3 xenografts excised from the athymic nude mice.

TABLES

Supplemental Table 1 – ERβ and ERα binding affinities and K_i values of FHNP, as compared to estradiol. Competitive assays on the purified ligand binding domains of ERβ and ERα were performed using 23.8 nM ^{3}H-Estradiol as tracer. IC_{50} values represent the average of a single experiment performed in duplicate. K_i values were calculated from the IC_{50} values using the Cheng-Prusoff equation.

	Relative binding affinity (%)			**K_i (nM)**		
	ERβ	**ERα**	**β/α**	**ERβ**	**ERα**	**β/α**
Estradiol	100	100	1.0	0.09	0.02	0.22
FHNP	5.2	1.5	3.5	1.83	1.59	0.87

Supplemental Table 2 – Biodistribution 1 h after intravenous injection of ^{18}F-FHNP in mice bearing a SKOV3 tumor. Competition studies were performed by injection of the tracer with either estradiol (non-selective, 0.3 µg/g animal, i.v.) or genistein (ERβ-selective, 5 µg/g animal, i.p.). Data are expressed as %ID/g (mean ± standard deviation). Statistically significant differences between treated and control animals are indicated by asterisks: * for $p<0.05$ and ** for $p<0.001$.

Organ	**Control (n=6)**	**Estradiol (n=5)[a]**	**Genistein (n=4)[a]**
Bone	0.49± 0.35	0.47± 0.14	0.49±0.16
Brain	0.05±0.03	0.04±0.01	0.08±0.07
Fat	0.39±0.27	0.54±0.37	0.18±0.12
Heart	0.28±0.13	0.38±0.32	0.38±0.04
Kidney	2.20±1.09	1.77±0.34	3.42±2.03
Liver	3.33±1.03	3.59±1.68	2.81±0.40
Lung	1.58±0.27	2.17±1.14	2.79±0.72*
Muscle	0.10±0.02	0.14±0.07	0.14±0.04
Plasma	1.05±0.12	1.48±0.44[b]	1.55±0.23*
Red blood cells	0.50±0.10	0.88±0.49	0.93±0.26*
Spleen	0.35±0.11	0.32±0.05	0.49±0.14
Prostate	3.42±3.93	2.96±1.66	1.84±0.95
Tumor	0.57±0.07	0.45±0.10*	0.30±0.08**
Urine	103.9±58.8	100.7±60.4	117.2±79.9

[a] 3 animals were excluded from the experiment due to the failure in either tracer or blocker injection

[b] One plasma value was excluded since it was an outlier according to the Grubbs' test.

Supplemental Table 3 – Biodistribution 1 h after intravenous injection of ^{18}F-FES in mice bearing a SKOV3 tumor. Competition studies were performed by injection of the tracer with either estradiol (non-selective, 0.3 μg/g animal, i.v.) or genistein (ERβ-selective, 5 μg/g animal, i.p.). Data are expressed as %ID/g (mean ± standard deviation). Statistically significant differences between treated and control animals are indicated by asterisks: * for $p<0.05$.

Organ	**Control (n=6)**	**Estradiol (n=5)[a]**	**Genistein (n=6)**
Bone	0.74± 0.39	0.25± 0.13	0.36± 0.17
Brain	0.42±0.41	0.19±0.12	0.24±0.08
Fat	0.48±0.30	0.97±0.65	0.38±0.20
Heart	0.40±0.22	0.39±0.28	0.35±0.14
Kidney	2.71±1.74	2.66±1.91	2.62±1.11
Liver	5.19±2.81	4.53±2.31	4.43±1.61
Lung	0.82±0.54	0.67±0.64	0.72±0.41
Muscle	0.49±0.17	0.31±0.16	0.37±0.12
Plasma	1.18±0.55	1.11±0.57	1.08±0.37
Red blood cells	0.36±0.12	0.52±0.30	0.50±0.18
Spleen	0.76±0.39	0.36±0.25	0.72±0.21
Prostate	4.30±2.83	3.25±0.58	4.91±4.44
Tumor	1.32±0.66	0.56±0.35*	1.11±0.39
Urine	37.1±25.7	41.2±19.5	19.9±5.6

[a] one animal was excluded due to failure in the tracer injection.